48th AIAA/ASME/ASCE/AHS/ASC Structures, Structural Dynamics, and Materials Conference
 15th
23 - 26 April 2007, Honolulu, Hawaii

AIAA-2007-2311

Structural Optimization with Probabilistic Fracture Constraints in the Multidisciplinary Radome Optimization System (MROS)

Myles L. Baker* and Kevin M. Roughen †
M4 Engineering, Signal Hill, California, 90755

and

Bruce E. Moylan ‡ and Gerald W. Russell §
U.S. Army Aviation and Missile Research Development and Engineering Center, Redstone Arsenal, AL, 35898

Radome design presents a highly coupled problem that is well suited for a multidisciplinary approach. The Multidisciplinary Radome Optimization System (MROS) has been developed to provide a capability to improve the radome design process. Unlike many aerospace structures, radome material selection is driven by design considerations other than structural performance. As such, structural analysis of radomes is often conducted on brittle materials with significant dispersion in strength. To accurately determine the reliability of brittle radome structure, a probabilistic fracture analysis method is implemented in MROS. This probabilistic fracture analysis is incorporated in to a structural optimization routine for use in multidisciplinary optimization within MROS.

I. Introduction

Successful design of high performance, low cost, missile radomes clearly requires the capability to tailor electrical performance, analyze high-speed aerodynamics and aerothermodynamics, and ensure the structural integrity under extreme thermal and hydrometeor environments of materials that are not structurally optimal. What is less readily apparent is that these analyses are tightly coupled and the interactions among them cannot be neglected. While the traditional engineering approach separates analyses into disciplines, rapid design and optimization demands that analyses be performed in a multi-disciplinary manner. In order to achieve better, more capable vehicles, the failure to achieve an early and accurate representation of the physics within and among disciplines will result in failure of the program.

A traditional barrier to multi-disciplinary analysis has been the time involved with passing data between analyses of different disciplines. In fact, many processes in the past have required input from the engineer for the modeling of all interactions between disciplines. This invariably takes a significant amount of time, and is often infeasible for use early in the design process or for processes requiring iteration. Recently, significant advances have been made in the development of automated systems that perform integrated analysis. An excellent example of such a system is the Integrated Hypersonic Aeromechanics Tool (IHAT).[1] With the use of IHAT, an engineer can perform a multi-disciplinary analysis in which the vast majority of time is invested in the analyses within the disciplines. In addition to this streamlined analysis capability, IHAT offers a broad range of optimization techniques through the inclusion of the DAKOTA (Design Analysis Kit for Optimization and Terascale Applications) toolkit.[2] This allows the engineer to gain an understanding of the physics of the problem early in the design process that would not have been feasible in the past.

The Multidisciplinary Radome Optimization System (MROS) has taken the multidisciplinary approach and the optimization capability present within IHAT and focused them on the radome design problem. Noteworthy capabilities of the MROS system relative to IHAT include: electromagnetic performance analysis, incorporation of

* Chief Engineer, 2161 Gundry Avenue, Associate Fellow AIAA.
† Senior Engineer, 2161 Gundry Avenue, Member AIAA.
‡ Senior Aerothermodynamics Engineer, AMSRD-AMR-PS-PI.
§ Senior Thermal Analyst, AMSRD-AMR-PS-PI, Senior Member AIAA.

solid thermal and structural models, and probabilistic fracture analysis. Probabilistic fracture analysis is included in MROS due to the fact that many radomes are constructed from ceramic materials which are brittle and have significant dispersion in strength. This paper describes the MROS system in overview (including all disciplines considered), with special attention paid to the structural analysis details.

II. MROS System Overview

The most important step in defining the overall process is identifying what data is to be shared among the modules. This data passing was defined relatively early in the project and is shown in the Design Structure Matrix (DSM) diagram shown below.

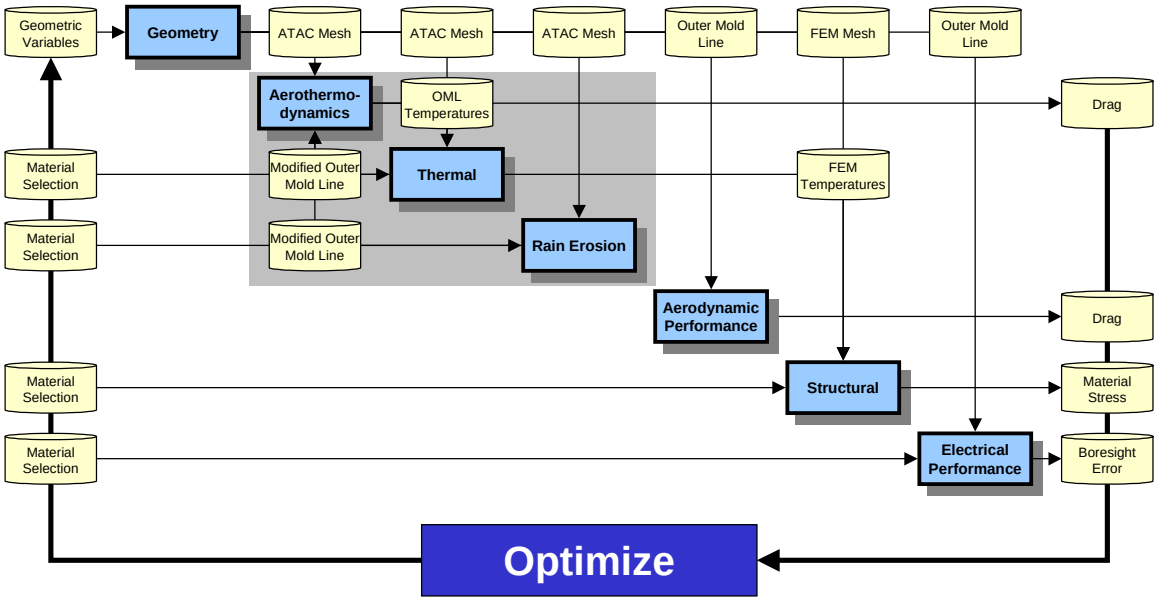

FIGURE 1: MROS DESIGN STRUCTURE MATRIX

A. Electromagnetics Module

The current electromagnetics module is based on a ray-tracing method that is valid for relatively high frequency radar/radome combinations. The method calculates the radome losses (copolarized and crosspolarized) and boresight error as functions of antenna azimuth and elevation for a monopulse antenna mounted in an axisymmetric multi-layer radome. The theory is based on geometric optics, which is essentially a ray-tracing approach that is valid as long as the size of the radome is large relative to the operating wavelength ($d \geq 10\lambda$). The Module calculates the boresight error (milliradians) in both the azimuth and the elevation channels as well as the copolarized and crosspolarized radome loss (decibels). Currently the geometry is limited to axisymmetric configurations, but modifications are underway to support arbitrary geometry. The software is also currently being enhanced to account for the effects of blockage due to a metallic nose tip. A boresight error result for a 3-layer radome (Fig. 2) and a textbook validation (Fig. 3) are included to illustrate typical MROS electromagnetic results.

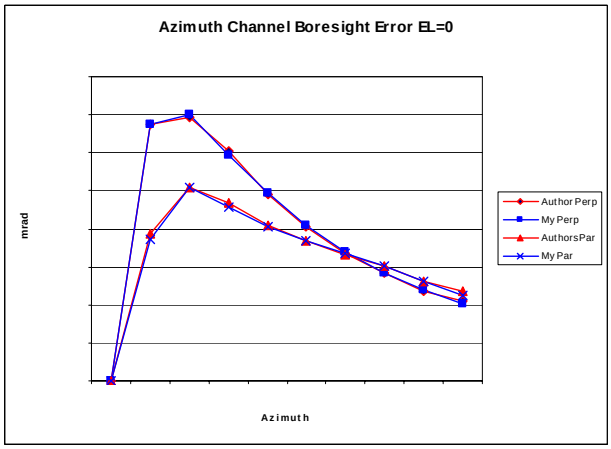

FIGURE 2: AZIMUTH AND ELEVATION BORESIGHT ERROR FOR THREE LAYER RADOME.

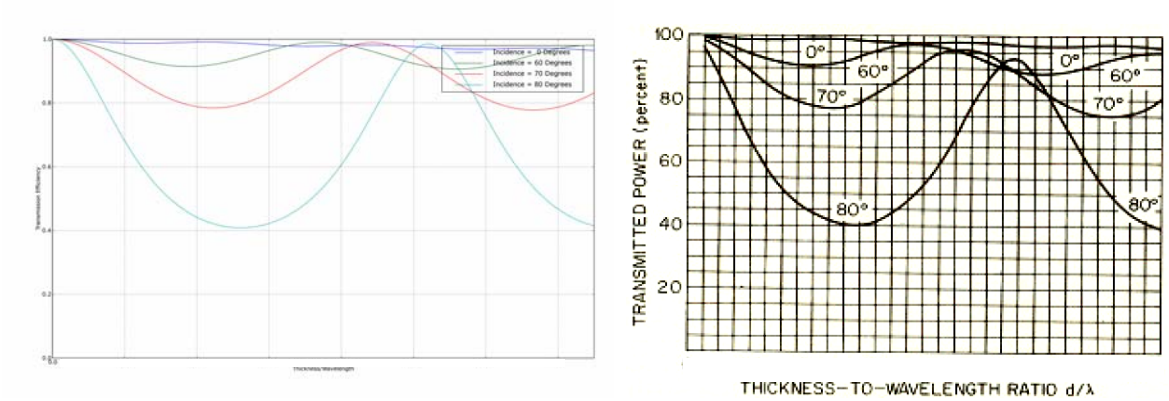

FIGURE 3: MROS TRANSMISSION EFFICIENCY COMPARES WELL TO REFERENCE RESULTS FOR A SLAB WITH ε=1.2, δ=0.003, PERPENDICULAR POLARIZATION. MROS DATA AT LEFT, REFERENCE DATA FROM [3].

B. Structural Module

The Structural Module is described in detail in Section III below.

C. The Aerothermodynamics Module

The Aerothermodynamics Module of the MROS is developed around the Aeroheating and Thermal Analysis Code (ATAC). ATAC provides the MROS user with extensively validated viscous and inviscid analysis based on the axisymmetric analogy offering substantially reduced analysis time relative to conventional CFD. In addition, MROS, with the use of ATAC can solve complex high altitude heat transfer and sheer stress models.

The Verification and Validation efforts of the MROS software have included comparison of aeroheating results to a classical solution. The heat flux for a hemispherical body has been computed for varying speed and altitude and is shown against data from Ref 4 in Fig 4 below. Excellent correlation in heat is observed including in the high speed regime where simplifications in the ideal gas method used in Ref 4 leads to overprediction of recovery temperature and underprediction of heat transfer coefficient.

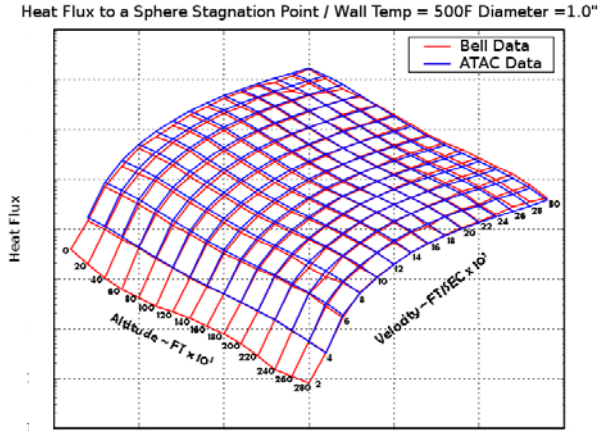

FIGURE 4: HEAT FLUX VALIDATION

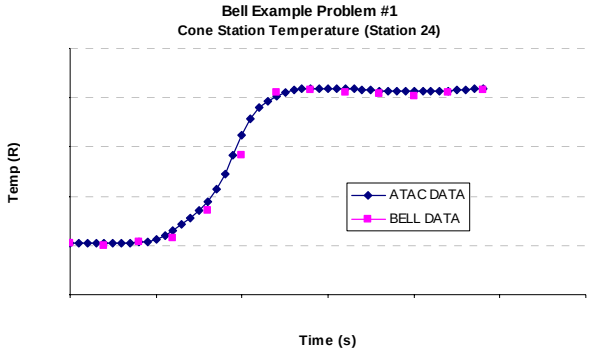

FIGURE 5: WALL TEMPERATURE VALIDATION

D. The Thermal Module

Multiple options for conduction analysis are present within MROS. For problems well characterized by 1-D conduction, the capability present within ATAC adequately predicts the temperature distribution. This capability is based on Aerotherm Charring Material Thermal Response and Ablation Program (CMA). This code has been extensively validated, and correlates well with existing data (Fig. 5).

For the nose region of radomes, accurate prediction of the temperature distribution is only achieved through 2-D or 3-D analysis. This is significant as this is often the critical region. MROS currently makes use of parametric FEM capability described in the structures section below to generate models capable of predicting the complex temperature distributions in radome nose regions. The thermal module maps the distributed heat transfer coefficient

and recovery temperature data from ATAC onto the FEM. Transient conduction analysis is then performed within Nastran.

E. Rain Erosion Module

The Rain Erosion Module of the MROS incorporates the rain erosion capability of ATAC. ATAC will provide the MROS user with validated procedures for different types of hydrometeor environments based on the data that is available to the user. The use of ATAC will account for rain, small snow, large snow, and ice. Distribution functions for each type of hydrometeor environment can be selected from the suggested average distribution functions as given by the Air Force Geophysics Laboratory or collected data can be inputted to obtain a more realistic result.

III. Radome Structural Analysis

The Structural Module assesses structural integrity based on aerodynamic heating and pressure data. In the current version of the system, the aerodynamic data is taken as input from ATAC. In order to calculate the probability of failure for the radome structure, the Structural Module generates a Finite Element Model, performs conduction analysis, structural analysis, and statistical fracture analysis and optimization. These analyses are described in detail below.

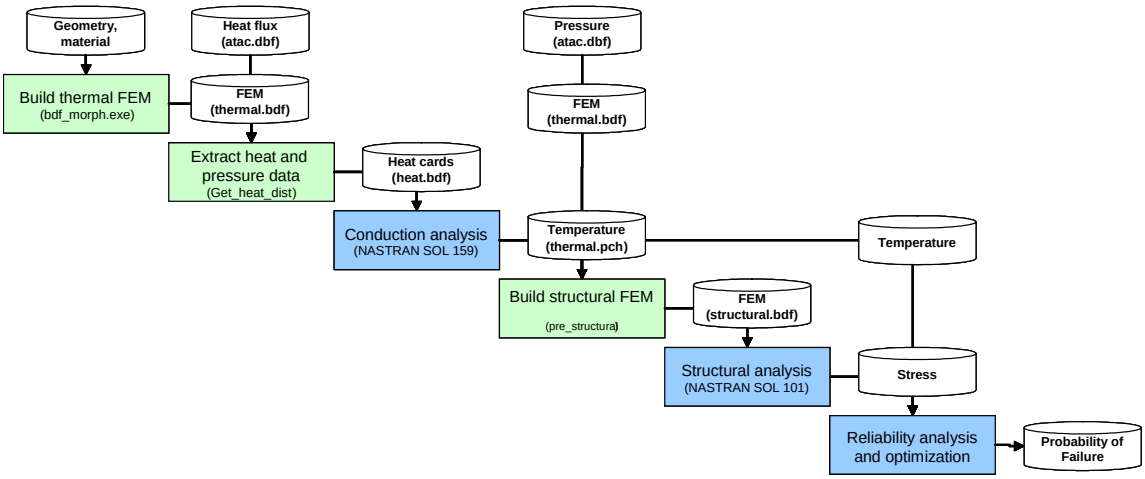

FIGURE 6: STRUCTURAL MODULE PROCESS.

A. Finite Element Model Morphing

The primary method of updating the radome configuration within MROS is through FEM morphing based on a library of baseline models. Geometric parameters such as length, base diameter, and nosetip radius are input by the user, from which target morphing volumes are generated. Morphing software then updates the FEM based on differences from the baseline morphing volumes, which are generated beforehand and are included in the MROS example library. Additionally, the morphing capability has significance for optimization. The ability to view the effects of minor alterations to geometry allows for simple optimization of design parameters. The integration of morphing code in MROS simplifies modifications to the FEM, and thus streamlines the optimization process. The use of morphing based on an existing FEM library enables appropriate handling of tip and base details. These details are represented in the baseline configuration, and with proper selection of the morphing scheme, are updated with design variations.

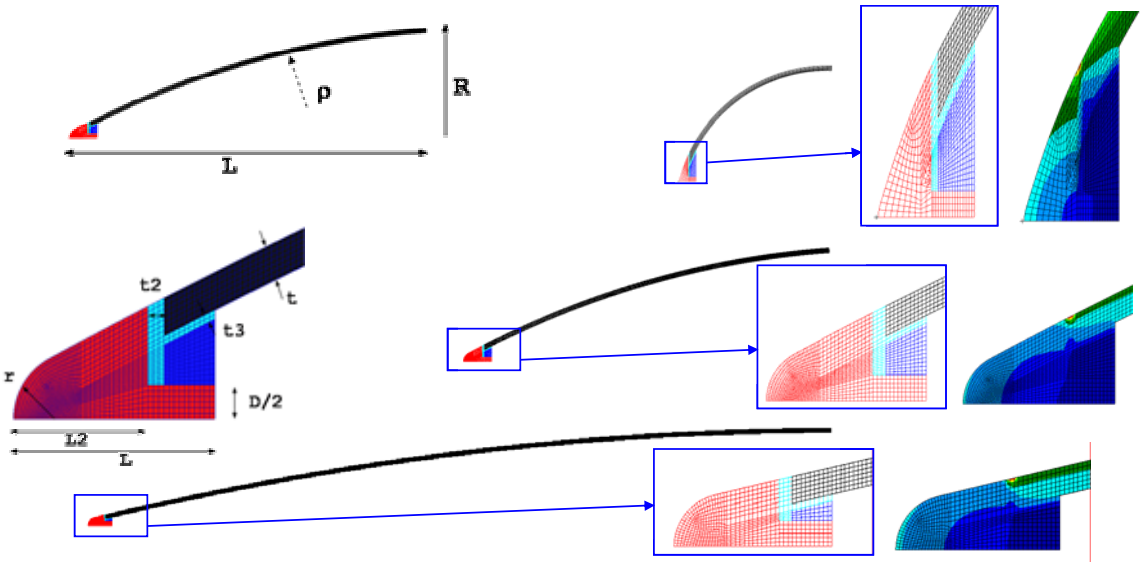

FIGURE 7: PARAMETRIC FEM GENERATION.

B. Stress Analysis

The stress analysis performed in MROS is relatively straightforward. Using the detailed FEM, the pressure distribution from the ATAC result, and the temperature distribution from the Nastran conduction solution a stress analysis is performed in Nastran. Currently this is performed as a linear static analysis. The use of the detailed FEM and temperature distribution allows for prediction of the stress distribution including local stress concentrations. It should be noted that the options selected in the design handbook portion of the FEM generation process determine the boundary conditions of the FEM and can have a significant impact on the results.

C. Statistical Fracture Mechanics

For applicability to brittle materials, the Structural Module includes a statistical fracture mechanics capability to the Finite Element results.

Using the data calculated in conduction and structural analyses, the statistical fracture mechanics module uses the Weibull two-parameter formulation. This expresses the volume and surface survival probability in terms of the stress distribution and material properties as:

$$P_{sV} = \exp[-\int_V (\sigma / \sigma_{oV})^{m_V} dV]$$

and

$$P_{sS} = \exp[-\int_A (\sigma / \sigma_{oS})^{m_S} dA].$$

In order to test the SFM Module, a simple test case from Reference 5 has been used. In order to be consistent with the example in Reference 5, SI units have been used in this example case. This model is essentially a beam in pure bending in the x-y plane. The finite element model used in the calculation is shown in Figure 7. This model has 40,000 HEX elements and 45,552 nodes. Note the use of a rigid element (purple) on the free (right) end of the beam to provide a load introduction path.

The beam is 1.0 mm thick (in the z direction), 4.0 mm high (in the y direction), and 10.0 mm long (in the x direction). The characteristic strength of the material is σ_{0v}=362.4 MPa-mm$^{0.2}$, and the Weibull modulus is m=15. The applied moment is 837.75 N-mm.

The resulting finite element stress results (maximum principal stress) are shown in Figure 7. Note that the upper half of the beam is in compression, so the maximum principal stress is approximately zero. The maximum stress from the finite element calculation is 314 MPa.

A simple hand calculation predicts a maximum stress of

$$\sigma = \frac{Mc}{I} = \frac{6M}{bh^2} = \frac{6 \times 837.75}{1.0 \times 4.0^2} = 314.16MPa$$

Showing excellent correlation with the finite element model.

An analytical prediction of the failure probability can be obtained by inserting the maximum principal stress into the failure equation. The maximum principal stress at any point in the beam is given by

$$\sigma = \begin{cases} 0 & y > 0 \\ -12My / bh^3 & y \le 0 \end{cases}$$

The integral in the failure probability equation can then be expressed as

$$\int_V \left(\frac{\sigma}{\sigma_{0v}} \right)^m dV = \int_{-b/2}^{b/2} \int_0^L \int_{-h/2}^0 \left(\frac{-12My}{bh^3 \sigma_{0v}} \right)^m dydxdz$$

Which can be simplified to give

$$\int_V \left(\frac{\sigma}{\sigma_{0v}} \right)^m dV = \frac{bLy}{m+1} \left(\frac{-12My}{bh^3 \sigma_{0v}} \right)^m \Bigg|_{-h/2}^0 = \frac{bLh}{2(m+1)} \left(\frac{6M}{bh^2 \sigma_{0v}} \right)^m$$

Substituting in the values for the parameters, we calculate a value of the integral of 0.14664. This results in a probability of failure of 0.136399.

The FEM-based statistical fracture module calculates a probability of failure of 0.13327, which is considered to be an excellent comparison with the theoretical value.

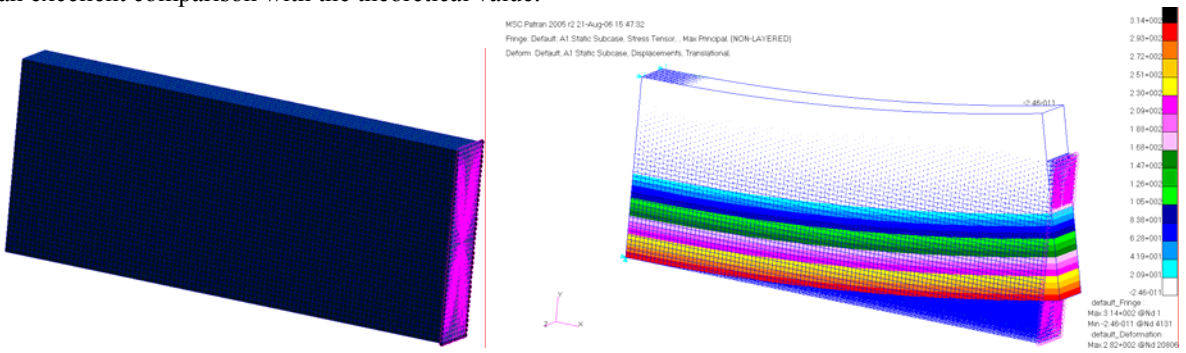

FIGURE 8: MAXIMUM PRINCIPAL STRESSES AND DEFORMATIONS CALCULATED BY NASTRAN SHOW EXCELLENT AGREEMENT WITH HAND CALCULATION.

In order to determine the survival probability over a mission, the Structural Module considers the greatest probability of failure for each element across all of the times analyzed. This is then summed to obtain the overall probability of failure.

IV. Secant Ogive Example Problem

Example problems will be essential for Verification, Validation, and Accreditation (VV&A) of MROS, as well as for defining which capabilities are valuable for the system. Several sample problems for preliminary code testing will be available, including flat plate and hemispherical radomes. The first realistic sample problem is a ceramic tangent ogive with an insulated refractory metal nosetip.

A. Problem Definition

The finite element model used as an example problem was generated with 2D elements modeling a majority of the structure aft of the nosetip in order to decrease computational requirements. The nosetip FEM contains material regions corresponding to metal, insulator, and ceramic. Analysis has been conducted along a representative flight trajectory.

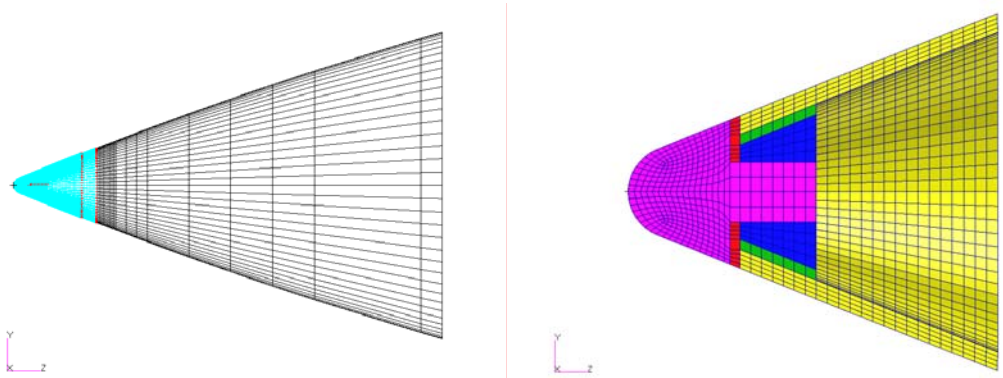

FIGURE 9: EXAMPLE RADOME FEM AND NOSETIP CROSS-SECTION

B. Results

The example problem is analyzed in the MROS system over a hypersonic trajectory. Temperature plots for the example problem are shown in Figure 10. The peak temperature in the radome is at the nose tip, with high temperature present through the insulator and at the ceramic material. The peak stress in the ceramic material is located at the inner forward edge of the dome. This stress is driven the thermal expansion of the insulating material. The probability of failure in the ceramic material is determined to be 0.0026% when integrated over the trajectory.

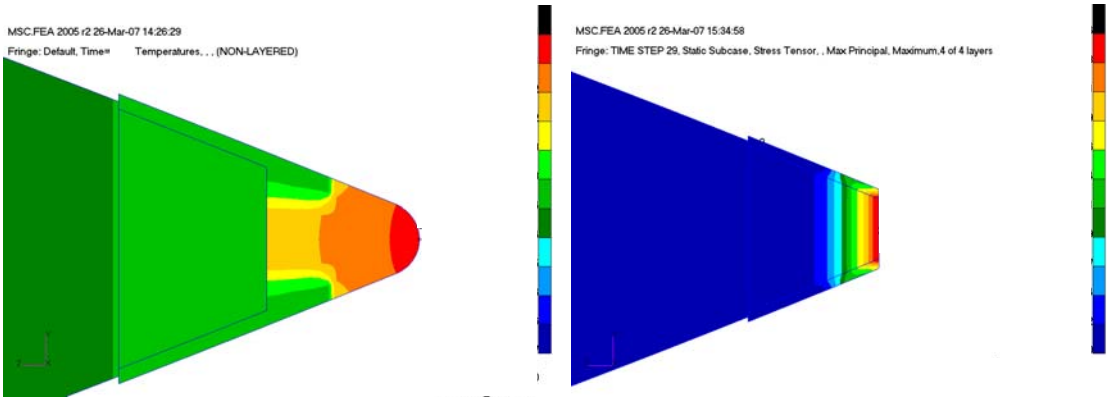

FIGURE 10: EXAMPLE RADOME TEMPERATURE AND STRESS RESULTS

V. Optimization Example Problem

A. Initial Optimization

Initial verification and validation of the optimization capability has been performed on the notional secant ogive example problem. In order to create a demonstrative example problem with minimal computer runtime, a simple set of design requirements and objectives were used. In order to meet these requirements and objectives, MROS was given access to radome length and wall thickness as design variables.

Requirements:

- Ceramic secant ogive radome operating at constant frequency with constant base diameter
- Wall thickness greater than constraint value (notional rigidity constraint)
- Structural weight less than constraint value

Objectives:

- Minimum drag
- Minimum straight-ahead copolarized transmission loss (at operating frequency)

Design Variables

- Radome length
- Wall thickness

While a more representative design problem has been left for future work, this problem does provide sufficient performance and constraint tradeoffs to present a viable optimization problem. Minimization of wall thickness minimizes weight, while wall thickness at a multiple of half wavelengths will minimize transmission loss. Minimization of radome length minimizes weight while maximization of radome length minimizes drag.

Optimization has been performed using a Genetic Algorithm with two weighting function vectors on the design objectives. These solutions are referred to as the loss weighted and drag weighted optimizations. The results of these optimization runs are shown in the figure below. Note that hollow data points represent infeasible solutions (weight greater than the constraint) while solid data points represent feasible solutions. Data points gathered from the loss weighted optimization are denoted with red squares, while data points gathered from the drag weighted optimization are denoted with blue diamonds. The optimum point from each optimization is circled. The results correlate well with an engineering understanding of the design space presented to the optimizer. The trend of the approximate Pareto Frontier shows that as the weighting on drag is increased, solutions with increased loss are selected. Drag weighted solutions have increased length requiring decreased thickness to satisfy the weight requirement. This decrease in thickness deviates from a half wavelength wall thickness and results in increased transmission loss.

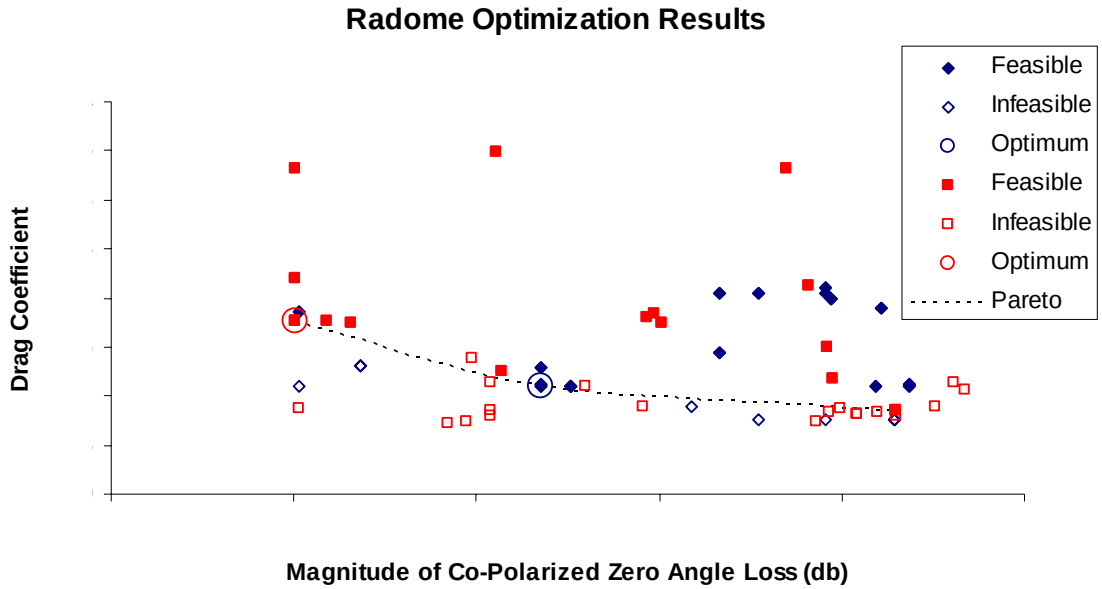

FIGURE 11: OPTIMIZATION RESULTS PLOTTED AS DRAG VS LOSS (RED SQUARES ARE LOSS WEIGHTED, BLUE DIAMONDS ARE DRAG WEIGHTED) (APPROXIMATE PARETO FRONTIER IS INCLUDED AS DASHED LINE)

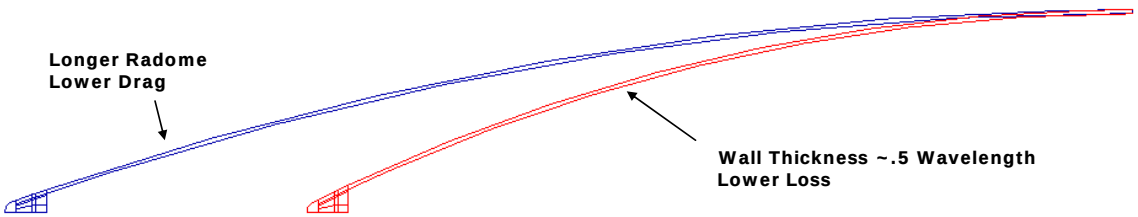

FIGURE 12: GEOMETRY OF OPTIMA FROM LOSS WEIGHTED (RED RADOME) AND DRAG WEIGHTED (BLUE RADOME) OPTIMIZATIONS

B. Optimization Including PFM

Inclusion of probabilistic fracture mechanics constraints in the optimization problem will lead to a more representative example. Design variants such as decreased tip radius and increased length that decrease drag, while increasing heating (and thereby probability of failure) will be included and will lead to improved understanding of the design space. Optimization with PFM is currently in work with the following design variables, requirements, and objectives.

Requirements:

- Ceramic secant ogive radome operating at constant frequency with constant base diameter
- Wall thickness greater than constraint value (notional rigidity constraint)
- Structural weight less than constraint value
- Probability of failure less than constraint value

Objectives:

- Minimum drag
- Minimum straight-ahead copolarized transmission loss (at operating frequency)

Design Variables

- Radome length
- Wall thickness
- Nosetip radius

VI. Conclusion

The MROS system provides a unique capability for high fidelity multidisciplinary analysis and optimization of radomes. This includes, Geometry, Aerothermodynamics, Thermal, Rain Erosion, Aerodynamic Performance, Structural, and Electromagnetic Performance. From a structural point of view, analytical capability includes calculation of stresses due to mechanical and thermal loads, and structural reliability (probability of failure) for ceramic materials. We expect MROS to be very useful in the design of future vehicle radomes.

VII. Acknowledgement

Funding for the development of MROS is provided by U.S. Army Aviation and Missile Research Development and Engineering Center, Redstone Arsenal. The authors also wish to acknowledge the contributions of the rest of the MROS team, without whose contributions this work would not be possible.

VIII. References

1. Baker, M.L., Munson, M.J., Hoppus, G.W., and Alston, K.Y., "Integrated Hypersonic Aeromechanics Tool (IHAT), Build 4," AIAA Multidisciplinary Analysis and Optimization Conference, Albany, NY Sept 2004.
2. Eldred, Michael S., Giunta, Anthony A., Hart, William E., van Bloemen Waanders, Bart G., and Wojtkiewicz, Steven F. Jr., "DAKOTA, A Multilevel Parallel Object-Oriented Rfamework for Design Optimization, Parameter Estimation, Uncertainty Quantification, and Sensitivity Analysis, Version 3.1 Users Manual," Sandia National Laboratories, Albuquerque, NM, April 2003.
3. Skolnik, Merrill, I., *Radar Handbook*, McGraw-Hill, New York, 1970.
4. Harms, Richard, J., and Schmidt, Craig, M., *A Manual for Determining Aerodynamic Heating of High-Speed Aircraft. Volume I*, Bell Aerospace Corp. Buffalo NY, June 1959.
5. Powers, L.M., Starlinger, A., and Gyekenyesi, J.P., Ceramic Component Reliability with the Restructured NASA/CARES Computer Program, NASA TM 105856, 37th ASME International Gas Turbine and Aeroengine Congress, Cologne, Germany, June 1-4, 1992.
6. Baker, M.L., Munson, M.J., Hoppus, G.W., and Alston, K.Y., "Weapon System Optimization in the Integrated Hypersonic Aeromechanics Tool (IHAT)," AIAA Multidisciplinary Analysis and Optimization Conference, Albany, NY, Sept 2004.
7. Nemeth, N. N., Manderscheid, J. M., Gyekenyesi, J. P., "Ceramics Analysis and Reliability Evaluation of Structures (CARES)", NASA Technical Paper 2916, August 1990.

8. “Users Manual for the Aeroheating and Thermal Analysis Code (ATAC03),” ITT Aerotech, Huntsville, AL, May 2003.
9. Thornton, E. A., Thermal Structures for Aerospace Applications, AIAA, 1996.
10. Bertin, J.J., Hypersonic Aerothermodynamics, AIAA, 1994.
11. Kozakoff, D.J., Analysis of Radome-Enclosed Antennas, Artech House, Inc. 1997
12. Jenn, D.C., Radar and Laser Cross Section Engineering Second Edition, AIAA, 2005
13. Hirsch, H.L., Grove, D.C., Practical Simulation of Radar Antennas and Radomes, Artech House, Inc., 1987
14. A. L. Murray, G. W. Russell, “Coupled Aeroheating/Ablation Analysis for Missile Configurations”, Journal of Spacecraft and Rockets, Vol. 39, No 4, April 2002.
15. J. D. Walton Jr., Radome Engineering Handbook-Design and Principles, Marcel Dekker Inc., New York. 1970.
16. Radome Engineering Handbook, Design & Principles, J.D. Walton Jr. Georgia Institute of Technology, ISBN 0-8247-1757-0, Marcel Dekker Inc New York 1970.
17. G. K. Huddleston, H. L. Bassett and J. M. Newton, "Parametric Investigation of Radome Analysis Methods" Final Report AFOSR-77-3469 Vol 1 of 4 Georgia Institute of Technology, February 1981.
18. G. K. Huddleston and A. R. Balius, "A Generalized Ray Tracing Method for Single-Valued Radome Surfaces of Revolution," Proc: 15th Symp on EM Windows, June 1980 pp 44-50.
19. R. Siwiak, T.B. Dowling and L.R. Lewis, "Boresight error induced by missile radomes," IEEE Tran: AP-27 No. 6, November 1979, pp. 832-841
20. T.E Tice (ed.), "Technique for airborne radome design," AFAL-TR-66-391, Vol. 1, Ch. 2, December 1966.
21. Practical Simulation of Radar Antennas and Radomes, Herbert L. Hirsch and Douglas C. Grove, Artech House, Inc. Norwood MA, ISBN 0-89006-237-4 1987.
22. Advanced Engineering Sciences Division, SRBSN Radome Summary, ITT Industries Inc., 2006